# United States
# Naval Postgraduate School

Monterey California
93940

12 Oct 1971 NPS-61Md71101A

## The Rough Surface and Bubble Effects on Sound Propagation in a Surface Duct.

H. Medwin

Ocean Physics Group
Physics Department

# The Rough Surface and Bubble Effect on Sound Propagation in a Surface Duct

by

Herman Medwin
Physics Department
Naval Postgraduate School, Monterey, California 93940

## ABSTRACT

Theories of rough surface scatter and gas bubble behavior are used with the Pierson-Moskowitz wind-wave spectrum and an empirically-guided formulation of bubble concentrations at sea to calculate the true velocity gradient and losses "at the surface". These values are then entered into Bucker's wave theory solution for sound propagation and leakage in a surface duct. Curves of propagation loss are calculated for comparison with ocean test data obtained with the SQS-26 sonar. The predictions are shown to be significantly better than those based on the empirical equations of project AMOS.

# I. INTRODUCTION

The purpose of this paper is to show that physical descriptions of bubble behavior and sound scatter at the sea surface, extended by laboratory experiments and in-situ measurements of near-surface bubbles have, at last, made it possible to give reasonably accurate predictions of surface duct propagation from a knowledge of wind speed over the surface and duct velocity profile.

We will start with a review of the current oceanographic description of the sea (Section II), and surface scattering theory (Section III), supplementing the basic formalism by the results of recent laboratory studies. The theory of sound dispersion, scatter and absorption by bubbles, simple bubble kinetics, the extrapolated results of in-situ near-surface bubble measurements are developed in Section IV.

(U) Finally (Section V), and with the very generous cooperation of Dr. Homer R. Bucker of the Naval Research Laboratory, who used his computerized wave guide solution[1] as a test for our surface loss and refraction predictions, we look again at the data of two SQS-26 propagation experiments performed by the Key West Test and Evaluation Detachment. Bucker's wave theory solution is modified by using the observed wind speed at the time of the experiment to correct the velocity gradient for bubble presence and to determine the bubble and surface losses which now replace an empirical one db surface loss factor that he used to obtain excellent data fits.

## II. THE SEA

We assume that the sea surface from which the sound is scattered is homogeneous, and that the temporal variation of sea heights, $\zeta$ , at a point is Gaussian distributed with mean value zero,

$$\langle \zeta \rangle = 0$$

and with variance, $\sigma^2$ ,

$$\langle \zeta^2 \rangle = \sigma^2$$

The surface height correlation function is

$$C = \frac{Z}{\sigma^2} = \frac{\langle \zeta(0,0,0)\, \zeta(u,v,\tau) \rangle}{\sigma^2} \qquad (1)$$

where u, v, $\tau$ are the spatial and temporal lags.

The Fourier transform of Z yields the three-dimensional spectrum of the sea

$$X(\varkappa_x, \varkappa_y, \Omega) = (2\pi)^{-3} \int_{\tau} \int_{u,v} Z(u,v,\tau) \exp\left[i(\varkappa_x u + \varkappa_y v - \Omega\tau)\right] du\,dv\,d\tau \qquad (2)$$

where $\varkappa_x, \varkappa_y$ = components of surface wave propagation constant

$\Omega$ = angular frequency of surface wave

We shall assume the gravity wave relation between angular frequency, propagation constant and acceleration of gravity, g:

$$\Omega^2 = \varkappa g ,$$

This permits the directional spectrum of the sea to be specified either in the two-dimensional rectangular coordinate form

$$X = \Psi(\varkappa, \alpha)\ \delta(\sqrt{g\varkappa} - \Omega) \tag{3a}$$

or the polar form,

$$X = \Psi(\varkappa_x, \varkappa_y)\ \delta(\sqrt{g\varkappa} - \Omega) \tag{3b}$$

where the Dirac delta function, $\delta(\sqrt{g\varkappa} - \Omega)$, simply selects the wave that fulfills the gravity wave relation between frequency and propagation constant.

The more commonly measured frequency spectrum $\Phi(\Omega)$ is now obtained by using the energy density coordinate transformation

$$\int_0^{2\pi} \Psi_K dK d\alpha = \Phi(\Omega)\, d\Omega$$

This permits the frequency spectrum to be expressed as the integral of the polar form of the $\varkappa$ spectrum over all azimuth angles,

$$\Phi(\Omega) = \frac{2\Omega^3}{g^2} \int_0^{2\pi} \Psi(\varkappa, \alpha)\, d\alpha \tag{4}$$

The semi-empirical form of the frequency spectrum for the fully-developed sea that is most widely accepted today[2] (Pierson-Moskowitz) is

$$\Phi(\Omega) = \frac{\alpha g^2}{\Omega^5} \exp\left[-\beta\left(\frac{\Omega_o}{\Omega}\right)^4\right] \tag{5}$$

where

$\alpha$ = $8.1 \times 10^{-3}$

$\beta$ = 0.74

$\Omega_o$ = $g/W_{19.5}$

$W_{19.5}$ = Wind speed at 19.5M above sea surface

$g$ = acceleration of gravity in consistent units

The three statistical parameters of the sea surface that are most significant in specifying the sound scatter are the mean square suface height, $\sigma^2$, the mean square surface slope, $\Sigma^2$, and the surface height correlation function, C.

For a locally-generated sea we obtain the mean square height by integrating the frequency spectrum for the fully-developed sea, Eq. (5):

$$\sigma^2 = \int_o^\infty \Phi(\Omega)\, d\Omega = \frac{\alpha W^4}{4\beta g^2} \qquad (6)$$

For the mean square slope, it is convenient to use the relation determined from optical measurements of the sea[3]

$$\Sigma^2 = 5.12 \times 10^{-5} W_{41} + 0.003 \pm 0.004 \qquad (7)$$

where $W_{41}$ is measured in cm/sec at a height of 41 feet over the surface. Unfortunately the measured speed is sensitive to the height of the anemometer; however corrections can be made.[4]

Finally, for simplicity and because of the general lack of two-dimensional sea correlation data, we will assume that the spatial correlation function is of Gaussian form and isotropic:

$$C(\ell) = e^{-(\ell/L)^2} \tag{8}$$

where

$$\ell = \sqrt{u^2 + v^2}$$

and $L \equiv$ surface correlation length.

The assumption of an isotropic Gaussian function makes it possible to calculate the correlation length from a knowledge of rms slope, $\Sigma$, and rms height, $\sigma$, by the relation that is valid for seas of lesser roughness :

$$\Sigma = \sqrt{2}\,\frac{\sigma}{L} \tag{9}$$

## III. SOUND SCATTERING THEORY AND LABORATORY STUDIES

The theoretical solution to the sea surface sound scattering problem usually starts with the Helmholtz Integral:

$$p_Q = \frac{1}{4\pi} \int_S \left[ \frac{e^{ikr_2}}{r_2} \frac{\partial p}{\partial n} - p \frac{\partial}{\partial n} \left( \frac{e^{ikr_2}}{r_2} \right) \right] dS \qquad (10)$$

where $p_Q$ = the scattered acoustic pressure at an interior field point, Q, of an enclosed volume.

$S$ = integrating surface selected so that acoustic field is zero everywhere except on the ensonified water surface.

$k$ = $2\pi/\lambda$ = acoustic propagation constant

$\lambda$ = acoustic wave length in water

$r_2$ = distance from surface scattering region to field position.

$n$ = normal to surface scattering point.

See Figure 1.

After applying the boundary conditions for acoustic pressure and acoustic particle velocity at the sea surface, and assuming that there is no shadowing or secondary scattering even for near-grazing incidence, we obtain the integral for the scattered pressure (now called $\Delta p_2 \equiv p_Q$) from a given surface of scattering area $\Delta A$ in terms of the geometry:

$$\Delta p_2 = \Delta p_{2_{plane}} \frac{F}{\Delta A} \int_{\Delta A} e^{i(\underline{k}_1 - \underline{k}_2) \cdot \underline{r}} dS \qquad (11)$$

where $\Delta p_{2_{plane}}$ = scattered pressure for a plane surface $\Delta A$ over which there is negligible curvature of the incident wave front.

$$= ik p_i \Delta A \cos\theta_1 \, e^{ik(r_2 - \omega_i t)}/2\pi r_2$$

$\Delta A$ = ensonified surface area over which $p_i$ is constant and the sagitta of the wave front is less than $\lambda/8$ .

$p_i$ = incident sound pressure at sea surface.

$\omega_i$ = incident sound angular frequency

$$F = \frac{1 + \cos\theta_1 \cos\theta_2 - \sin\theta_1 \sin\theta_2 \cos\theta_3}{\cos\theta_1 (\cos\theta_1 + \cos\theta_2)}$$

$\theta_1$ = angle of incidence (measured with normal)

$\theta_2$ = angle of scatter (measured with normal)

$\theta_3$ = azimuthal angle of scatter plane with respect to incident plane.

$\underset{\sim}{k}_1 = k (\underset{\sim}{i}_1 \sin\theta_1 - \underset{\sim}{i}_3 \cos\theta_1)$

$\underset{\sim}{k}_2 = k (\underset{\sim}{i}_1 \sin\theta_2 \cos\theta_3 + \underset{\sim}{i}_2 \sin\theta_2 \sin\theta_3 + \underset{\sim}{i}_3 \cos\theta_2)$

$\underset{\sim}{i}_1, \underset{\sim}{i}_2, \underset{\sim}{i}_3$ are the unit normals in the x, y and z (depth) directions, respectively.

It should be noted that the solution being presented assumes that the illuminated surface is in a small section ($\sqrt{\Delta A} << r_1$) of the Fraunhofer region of the source field and that the field position is in the Fraunhofer region of the illuminated area ($r_2 \gg \sqrt{\Delta A}$, $r_2 >> \Delta A/\lambda$ ). This point is emphasized by our $\Delta$ notation for the illuminated area.

The mean square scattered pressure, which in general includes both coherent and incoherent sound intensity, is formulated:

$$\langle \Delta p_2 \Delta p_2^* \rangle = I_{pl} \frac{F^2}{(\Delta A)^2} \int_x \int_y \int_{x'} \int_{y'} \langle e^{iK_z[\zeta(x,y) - \zeta(x',y')]} \rangle e^{i[K_x u + K_y v]} \, (dx dx' dy dy')$$

where

$$\underline{K} = \underline{k}_1 - \underline{k}_2$$

$$u = x' - x$$

$$v = y' - y$$

$$I_{pl} = \Delta p_2{}_{plane} \; \Delta p_2{}^*{}_{plane}$$

$$* = \text{complex conjugate}$$

$$\langle\ \rangle = \text{ensemble average}$$

The ensemble average, $\langle\ \rangle$, can be easily evaluated for our surface with its two-dimensional Gaussian distribution:

$$\langle e^{iK_Z(\zeta - \zeta')} \rangle = e^{-[k\sigma(\cos\theta_1 + \cos\theta_2)]^2 [1 - C]}$$

Define the ACOUSTICAL ROUGHNESS OF THE SEA SURFACE $\equiv g$

$$g \equiv [k\sigma(\cos\theta_1 + \cos\theta_2)]^2 \qquad (12)$$

so that the mean scattered intensity can be written

$$\langle \Delta p_2 \Delta p_2{}^* \rangle = I_{pl} \frac{F^2}{(\Delta A)^2} e^{-g(1-C)} \int_x \int_y \int_{x'} \int_{y'} e^{i(K_x u + K_y v)} \, dx dx' dy dy' .$$

If our interests were to be restricted to low roughness ($g < 1$) at this point, it would be useful to use the approximation $e^{-g(1-C)} \simeq (e^{-g})(1+gC)$. This would permit immediate separation into a coherent term, $e^{-g}$, and an incoherent term which the integration would transform into the two dimensional surface spectral description, eqn. (3b) , (Weiner-Khinchine transformation).

The rarity of experimental measurements of two-dimensional surface spectral descriptions turns us away from this approach.

Instead, for scatter in the specular direction, it is convenient to try a series approximation to the assumed isotropic Gaussian spatial correlation function (Eq. 8). The integration[5,6] then produces the relative scattered intensity, (compared with the plane surface reflected intensity) specialized to specular scatter, in which $\theta_1 = \theta_2$, $\theta_3 = 0$, $F = 1$, $g = 4k^2\sigma^2 \sin^2\phi$ where $\phi = 90 - \theta_1$ = grazing angle.

$$\langle \rho\rho^* \rangle \equiv \frac{\langle \Delta p_2 \Delta p_2^* \rangle}{I_{plane}} = e^{-g} + \frac{\pi L^2}{\Delta A} \left( e^{-g} \sum_{m=1}^{\infty} \frac{g^m}{m!m} \right) \tag{13}$$

The two terms of Eq. (13) represent coherent scattered sound (the $e^{-g}$ term) and incoherent scattering (the second term). A study of the term in parentheses, defined as

$$S(g) \equiv e^{-g} \sum_{m=1}^{\infty} \frac{g^m}{mm!} \tag{14}$$

shows that $S(g) \to g$ for $g << 1$

and $S(g) \to \frac{1}{g}$ for $g >> 1$ .

Since it can be assumed that $L^2 < \Delta A$, we can conclude that, in the limits, the specular scatter for a Gaussian sea will be:

For Small Acoustical Roughness, $g << 1$: $\langle \rho\rho^* \rangle = e^{-g}$ (15)

For Large Acoustical Roughness, $g >> 1$: $\langle \rho\rho^* \rangle = \frac{\pi L^2}{g \Delta A} = \frac{\pi}{2k^2\Sigma^2 \Delta A \sin^2\phi}$ (16)

In practice the coherent term is dominant approximately up to $g \simeq 1$, and sometimes beyond that roughness, depending on the beam width. Fig. 2

shows the relative behavior as a function of acoustical roughness. It is seen that for small acoustical roughness, the intensity of specular scatter is the factor $e^{-g}$ times the mirror reflection , and the concept of a reflection coefficient is useful.

However, it is important to observe also that the value of dB loss per bounce is in general an inadequate, and in fact misleading, concept for the rough surface case. When $g \gg 1$ the specific value of the scattering area enters into the asymptotic value of $\langle \rho \rho^* \rangle$ which will therefore change from one bounce to the next as the sound wave continues to diverge and scatter.

When the Fraunhofer conditions are violated (large beam width) it is necessary either a) to add the scatter contributions from the several areas[10] $\Delta A$ or b) to re-solve the problem, assuming a diverging wave at the very beginning of the derivation.[7,8] The latter attack and its verification by laboratory model[8] show that for specular scatter from an exponentially* correlated surface there is virtually no difference between the Fraunhofer and Fresnel solutions if $g < 1$. However, for $g > 1$ the scattered intensity may be significantly greater than predicted by the single Fraunhofer solution. This is because, commonly, significant signal will exist over an area containing more than one $\Delta A$ as defined in our derivation.

Laboratory models have been used in order to supplement the capabilities of current theory.[9,10] We have recently studied the behavior of the coherent component for cross-wind, up and down wind specular scatter under widely-varying laboratory seas. Our "seas" are produced by combinations of a paddle and five fans blowing air over the surface of our 25' x 6' x 8' deep anechoic tank. In this way we obtain water waves that give us scaled replicas of compound sea and swell surfaces that are realistically time-varying, anisotropic, and near-Gaussian. The probability density function, spatial and temporal correlations

*The Gaussian correlated surface would give similar results.

and frequency spectrum compare closely to ocean measurements[10], except for scale factors for frequency, time and space lag, of course.

Figure 3 shows three of the laboratory sea and swell spectra. The probability density functions of the wave height for the three cases are shown in Fig. 4; the near-Gaussian probability density function is very close to that observed at sea.[10] Equation (13) states that the ratio of the intensity of the coherent component to the intensity reflected from a mirror-like surface should be $e^{-g}$. Figure 5 shows this ratio divided by $e^{-g}$ over four decades of acoustical roughness; for $g \leq 1$ the ordinate is essentially unity. This excellent verification of theory, when tested under widely varying laboratory seas, has encouraged us to apply it to the real ocean. Other laboratory model results[11,12] suggest that for $g < 1$, at near grazing incidence, a shadowing correction is not necessary.

## IV. EFFECTS OF NEAR-SURFACE BUBBLES

Bubbles near the sea surface can modify the forward scatter of sound in two ways: (a) By near-surface refraction; the presence of all bubbles (resonant or not) will create a below-surface medium through which the speed of sound differs from that in the non-bubbly water; this change of speed will refract incoming rays, modify the angle of incidence at the rough-scattering surface and change the distance betweeen bounces in channel propagation. (b) By resonant absorption and scatter; resonant near-surface bubbles can cause attenuation that is generally unresolvable from rough surface scatter loss.

The objectives of the present work are arbitrarily restricted to "surface" losses at frequencies below 16 kHz. Nevertheless, because bubble refraction depends on the total volume of air in bubble form, it is necessary to consider the numbers of near-surface bubbles of all radii.

In spite of the great interest in the subject for almost 30 years, the literature of ocean bubble data is very thin: In-situ measurements of bubbles in off-shore breaking waves have been reported[13]; bubble generation and persistance by an artifical wind over a laboratory tank filled with sea water has been described[14]; inferred bubble densities have been calculated from certain AMOS data[15]; in-situ acoustical measurements in 60 ft of isothermal water in Mission Bay, San Diego have been summarized[16]; a laboratory study of surface bubbles has yielded data produced by colliding waves of sea water.[17] It will be necessary for us to extrapolate beyond these bare measurements available.

### A. Dependence on Radius

Because of experimental difficulties, in no case are there published in-situ measurements of ocean bubbles of radius greater than 200

microns (resonant frequency less than approximately 15 kHz) or less than roughly 20 microns (resonant frequency greater than 150 kHz). Most of the available data fit approximately the solid line in Fig. 6 , plotted on the basis of fractional volume of air in bubble form to water u(R)dR. From the fractional volume it is easy to calculate the number of bubbles per unit volume, in radius increment dR, by using

$$n(R)\, dR = \frac{u(R)\, dR}{4/3\pi R^3} \tag{17}$$

There is some evidence that the bubble populations break up roughly into two groups: those smaller than approximately 60 micron radius postulated as attached to motes and due principally to biological activity, cosmic rays, captured aerosols and photosynthesis of phytoplankton, and the larger bubbles which we assume come from breaking waves (and decaying matter on the sea floor in shallow water).

To calculate the near-surface refraction due to bubbles we have had to extrapolate (dashed lines) the data-based curves of Fig. 6, which were measured with incipient breaking waves at wind speeds 4-6 knots at 3.3 meter depth. For radii smaller than 30$\mu$ we extrapolate to one micron radius at the $K_2R^{-1/2}$ dependence that has been found for the smallest measured ocean bubbles[16] and in tap water[18]; below 1 micron, at slope $K_1R^0$ following behavior loosely suggested by laboratory cavitation studies.[19,20] For bubbles larger than 60$\mu$ we have used the $K_4R^{+1}$ dependence observed[14] to 100 microns and have

extrapolated to largest radii at Blanchard and Woodcock's slope of $K_5 R^{-3}$. The radius at which one shifts to the suggested slope for largest bubbles is, admittedly, somewhat arbitrary. That slope starts at about 50 microns in the breaking wave data; however, a re-analysis of Glotov's data shows that the $K_5 R^{-3}$ behavior is confirmed for $R > 120\mu$ . The constants for the slopes of Fig. 6 are shown in Table 1.

TABLE ONE

Estimated Fractional Bubble Air to Water at 3.3M depth for Winds Approximately 6 Knots

| Radius Range Microns | Dependence $u(R_0, 3.3M)$ | Constant [dimensions] | $\int u(R_0)\, dR$ |
|---|---|---|---|
| $R_0 \leq 1.0$ | $K_1 R_0^{0}$ | $K_1 = 1.5 \times 10^{-9}$ $[\mu^{-1}]$ | $1.5 \times 10^{-9}$ |
| $1.0 \leq R_0 \leq 30.$ | $K_2 R_0^{-1/2}$ | $K_2 = 1.5 \times 10^{-9}$ $[\mu^{-1/2}]$ | $13.8 \times 10^{-9}$ |
| $30. \leq R_0 \leq 60.$ | $K_3 R_0^{-1}$ | $K_3 = 8.5 \times 10^{-9}$ $[\mu^{0}]$ | $5.8 \times 10^{-9}$ |
| $60. \leq R_0 \leq 100.$ | $K_4 R_0^{+1}$ | $K_4 = 2.5 \times 10^{-12}$ $[\mu^{-2}]$ | $7.7 \times 10^{-9}$ |
| $100. \leq R_0$ | $K_5 R_0^{-3}$ | $K_5 = 2.5 \times 10^{-4}$ $[\mu^{+2}]$ | $12.4 \times 10^{-9}$ |

Total Effective $U = 4.1 \times 10^{-8}$

B. Dependence on Depth

For our purposes, interest lies in the bubble densities (and fractions) as a function of depth at a fixed frequency, rather than for fixed radius. Studies in well-mixed ocean water [16] suggest that for bubbles larger than approximately 30 microns (sea level resonant frequency less than 100 kHz) buoyant forces and turbulent entrainment determine the bubble life time rather than gas diffusion through the bubble walls. If we formally make the simplifying assumption that these bubbles can be lost only at the ocean surface, then bubbles of surface (3.3 Meter depth) resonant frequency $f_0$, radius $R_0$, will be found at depth Z in the same numbers, but at the isothermally* compressed radius, $R_{0Z} = R_0\beta^{1/3}$ and resonant frequency $f_{0Z}$ where $\beta = 1.33/(1 + 0.1Z)$.

For resonant air bubbles $kR_o = \frac{1}{c}\sqrt{\frac{3\gamma P}{\rho_o}}$ where $c \approx 1.5 \times 10^5$ cm/sec $\gamma = 1.4$, $P = 10^6\sqrt{1+Z/10}$ dyne/cm$^2$, $\rho_o \approx 1.0$ gm/cm$^3$, Z = depth in meters.

The bubble fraction at depth Z will be

$$u(R_{0Z},Z) = n(R_{0Z},Z)(4/3\ \pi R_{0Z}^3)$$

Analytically, our assumption for large bubbles is: from the surface to depths where the entrained bubble drag force is equal to or greater than the buoyant force

$$n(R_0,3.3M)\ dR = n(R_{0Z},Z)\ dR\ ,$$

*The restriction to "isothermal" waters is not severe, since small temperature changes will cause negligible volume changes.

so that following isothermal compression,

$$u(R_{0Z},Z) = [u(R_0,3.3M)][\beta]. \qquad (18)$$

These bubbles, however, have a resonant frequency which is not $f_0$, but, because of changed radius and pressure, is

$$f_{0Z} = f_0 \beta^{-5/6} .$$

We can now calculate the gas fraction of bubbles at the desired resonant frequency $f_0$ at depth Z, $u(f_0,Z)$, by assuming that the frequency dependence within a given band of bubble sizes is the same as at the surface, that is,

$$u(f_0,3.3M) = k_{n0} f_0^{\,n} \quad \text{and} \quad u(f_{0Z},Z) = k_{nZ} f_{0Z}^{\,n}$$

where n is the frequency dependence within a particular frequency band. Therefore

$$\frac{u(f_0,Z)}{u(f_{0Z},Z)} = (f_0/f_{0Z})^n = (\beta^{5/6})^n \qquad (19)$$

Finally, from (18) and (19)

$$u(f_0,Z) = (\beta^{5/6\ n+1})\ u(f_0,3.3M) \qquad (20)$$

and, taking account of the change in radius,

$$n(f_0,Z) = (\beta^{5/6\ n\ +\ 5/2})\ n(f_0,3.3M) \qquad (21)$$

The predicted depth dependences for the three most important bands of surface radii are shown in Table 2.

TABLE 2

Fractional Air in Bubble Form and Number of Bubbles per Unit Volume as a Function of Depth for Large Bubbles

| $R_0$ | $f_0$ | n | $u(f_0,Z)/u(f_0,3.3M)$ | $N(f_0,Z)/N(f_0,3.3M)$ |
|---|---|---|---|---|
| microns | kHz | | $= \beta^{5/6\ n+1}$ | $= \beta^{5/6\ n\ +\ 5/2}$ |
| 30 to 60 | 60 to 100 | +1 | $\beta^{11/6}$ | $\beta^{10/3}$ |
| 60 to 100 | 32 to 60 | -1 | $\beta^{1/6}$ | $\beta^{5/3}$ |
| > 100 | less than 32 | +3 | $\beta^{7/2}$ | $\beta^{5}$ |

It is clear that the assumptions that lead to the values in Table 2 can only be considered as a perturbation analysis of the change of bubble populations with depth since they imply inconsistencies, particularly at the edges of the bands, as depth is increased. Nevertheless, the only bubble density data available[16] plotted against the absolute pressure, $1.33\beta^{-1}$, for four frequencies between 40 and 96 kHz show slopes of approximately $\beta^{+2}$, in reasonable agreement with the predictions of $\beta^{1.7}$ to $\beta^{3.3}$.

When we plot the frequency band contributions to the total bubble fraction, ($\int u\ R\ dr$), as a function of total pressure parameter $\beta^{-1}$, the total bubble fraction U(Z) at wind speed 6 knots is found to vary (with less than 5% deviation) as $\beta^{+2}$ from the surface to approximately 10M depth, blending into $\beta^{+1}$ at greater depths (near 20 Meters). Therefore the dpeth dependence that we will use for the near-surface refraction calculation is:

$$U(Z) = 4.1 \times 10^{-8}\ \beta^{+2} \qquad (22)$$

C. Dependence on Wind Speed

It has been found [4] that the number of bubbles shows "an abrupt increase ... approximately ... exponential" for winds above about 6 knots. The comment agrees roughly with the curve of foam coverage vs. wind speed[21] which can be written approximately as:

$$U(Z=0,W) = U(Z=0,6 \text{ knots}) \left[1 + 10^{-2}(W/10)^2\right] \qquad (23)$$

where W = wind speed in knots.

There is a second wind effect: the larger, wind-generated bubbles will be brought to depths by increased turbulent entrainment. A complete knowledge of this behavior may be possible when there is a better understanding of underwater motion as a function of wind speed, insolation and depth.[22] However, the factor of bubble entrainment by water motion can be crudely evaluated by the following simple argument:

A bubble will be drawn down from the surface when the drag force is greater than the buoyant force.
The convective velocity in the medium will probably be Gaussian distributed. Nevertheless, the mean downward convective velocity will increase with wind speed as does the velocity spectrum[23] and the depth of the well-mixed layer.[24] We assume that the mean convective velocity is proportional to the wind speed and that the mean number of bubbles drawn downward under a given condition of underwater turbulence is proportional to the mean velocity; the dependence on radius will be ignored at this time. This "zero order" estimation of the effect of turbulent entrainment, combined with eq.(23) for the increased foam available leads to the wind dependence:

$$\frac{U(Z,R_0,W)}{U(Z,R_0,6 \text{ knots})} = (W/6)\left[1 + 10^{-2}(W/10)^2\right] \qquad (24)$$

D. Summary of Bubble Dependences

Combining the dependences on radius of bubble, bubble depth and wind speed, we get the total bubble fraction:

$$U(Z,W) = [4.1 \times 10^{-8} \beta^2] [W/6] [1 + 10^{-2}(W/10)^2] \qquad (25)$$

It is appropriate to point out that other bubble factors exist in addition to the effects that we have considered. Two significant elements are the dependence on daylight and precipitation; others are dependence on water temperature and gradient, percentage gas saturation, marine biological activity. As examples: Blanchard and Woodcock have shown that snow and rain produce very large numbers of bubbles. Their penetration in laboratory experiments was no more than 2 cm below the water surface but it would be expected that these bubbles would penetrate much farther in the presence of convection cells accompanying storms at sea. Small bubbles (less than about 60 $\mu$) are about twice as populous in the daytime as at night. It has been postulated that the increased numbers may be due to photosynthetic action.[16]

E. Theory of Dispersion and Absorption by Bubbles

Following classical developments [25] an incident acoustic pressure, of wave length very large compared to the bubble radius R, having a velocity potential $\psi_i e^{-i\omega t}$, will produce a total field

$$\psi(\mathbf{r}) = \psi_i(\mathbf{r}) + \sum_{n=1}^{N} \left(\frac{A_n}{r}\right) e^{ik|\mathbf{r} - \mathbf{r}_n|} \tag{26}$$

where $\mathbf{r}$ = coordinate position of scattering region

$\mathbf{r}-\mathbf{r}_n$ = distance between $n^{th}$ bubble and center of scattering region

$k = 2\pi/\lambda$ = propagation constant in bubble-free water

$$A_n = \frac{R\psi_n}{(\omega_o/\omega)^2 - 1 - i\delta}$$

$R$ = bubble radius

$\omega$ = incident sound frequency

$\omega_o$ = resonant frequency of bubble

$\delta$ = damping constant of bubble

The average over all possible sizes and configurations of bubbles is

$$\langle\psi(\mathbf{r})\rangle \approx \psi_i(\mathbf{r}) + \iiint G(\mathbf{r}_n)\ \langle\psi(\mathbf{r}_n)\rangle\ \frac{e^{ik|\mathbf{r} - \mathbf{r}_n|}}{|\mathbf{r} - \mathbf{r}_n|}\, dV_n \tag{27}$$

where

$$G(\mathbf{r}_n) = \int_R [n(\mathbf{r}, R)] \left[\frac{R\, dR}{[\omega_o(R)/\omega]^2 - 1 - i\delta(\omega, R)}\right]$$

(U) Equation (27) is the integral equation formulation of the differential equation

$$\nabla^2 \langle \psi \rangle + k^2 \langle \psi \rangle = -4\pi G \langle \psi \rangle \quad \text{or}$$

$$\nabla^2 \langle \psi \rangle + k_b^2(r) \langle \psi \rangle = 0 \tag{28}$$

where

$$k_b(r) = k\left[1 + \frac{4\pi G}{k^2}\right] \approx k + \frac{2\pi}{k} \int_R \frac{n(r,R)\, R\, dR}{(\omega_o/\omega)^2 - 1 - i\delta(R)}$$

The quantity, $\frac{k_b(r)}{k} = 1 + \frac{4\pi G}{k^2}$, is the index of refraction in the bubbly region. Because of the presence of the damping term, the index will have an imaginary part which comprises the attenuation due to absorption and scatter in the bubbly water in addition to the real part, defining the local speed of sound. These terms are:

$$\text{Re: } \{k_b(r)\} = k + \frac{2\pi}{k} \int_R \frac{R\, n(R)\left[\left(\frac{\omega_o}{\omega}\right)^2 - 1\right] dR}{\left[\left(\frac{\omega_o}{\omega}\right)^2 - 1\right]^2 + \delta^2} \tag{29}$$

$$\text{Im: } \{k_b(r)\} = \frac{2\pi}{k} \int_R \frac{\delta\, R\, n(R)\, dR}{\left[\left(\frac{\omega_o}{\omega}\right)^2 - 1\right]^2 + \delta^2} \tag{30}$$

F. Predictions of Refraction by Bubbles

The dispersion relation Eq. (29), since it predicts a decrease of sound speed caused by bubbles of resonant frequency greater than the incident frequency and an increase of speed for bubbles with lower resonant frequencies, would require precise information of bubble populations for an evaluation for all sound frequencies. However, if our interest is restricted to sound frequencies less than 16 kHz, integration of Fig. 6 shows that bubbles under that resonant radius ($R_0$ < 200. microns) represent approximately 93% of the total fractional air volume. For the calculation of refraction at frequencies less than 16 kHz we consider only the effect of bubbles of resonant frequency greater than the driving frequency.

When $\omega_o >> \omega$, we drop $\delta^2$ in the denominator of Eq. (29), use $\omega_o/\omega = R_o/R$ and the definition of u (R) to obtain the simplified form:

$$\text{Re:} \quad \{k_b\} = k\left(1 + \frac{3\,U}{2\,k^2\,R_o^{\,2}}\right) \qquad \omega << \omega_o \qquad (31)$$

Since the expression in parentheses is nearly unity, we find

$$c_b = c\left[1 - 8.0 \times 10^3\, U \quad (1 + Z/10)^{-1}\right] \qquad (32)$$

where U(Z,W) is given by equation (25).

The significance of this departure of the speed from the bubble-free value is evident when we insert Equation (25) and look at the gradient of the near-surface propagation speed. For the reference wind speed of 6 knots the gradient of the velocity, proportioanl to $(1 + 0.1Z)^{-4}$, has a surface value of 0.26 $sec^{-1}$, decreasing to 0.016 $sec^{-1}$ by 10 Meter depth. Since the velocity gradient due to pressure in isothermal water is 0.018 $sec^{-1}$ our conclusion must be that ray curvature in approximately the top 10 meters is very strongly influenced by bubbles even for winds as low as 6 knots.

Because of bubbles, rays approaching the surface will refract upward, meeting the surface in a cusplike ray path, and making more bounces for a given horizontal range than for a bubble-free region.

G. Predictions of Attenuation due to Bubbles

The sound pressure attenuation formula for the bubbly water can be written as

$$p = p_o \, e^{-\alpha x} \, e^{i(\omega t - k_b x)}$$

where $\alpha \equiv \text{Im: } \{ k_b \}$ .

Using Eq. (30) and rewriting in decibel notation, we get the attenuation

$$a_b = 8.68\,\alpha$$

$$= (8.68)\,(2\pi) \int_0^\infty \frac{(\delta/\delta_r)\, R^2 \; n(R,Z,W)\; dR}{\left[\left(\frac{\omega_o}{\omega}\right)^2 - 1\right]^2 + \delta^2} \qquad (33)$$

where $\delta_r$ = radiation damping constant = $k R_o$

$$\approx 1.36 \times 10^{-2} \sqrt{1+Z/10} \quad \text{for air bubbles}$$

Integration [26] yields

$$a_b = [8.68\pi^2 R_0^3 n(R_o,Z,W)]/\delta_r$$

which can be re-expressed as

$$a_b = 1.50 \times 10^9 \, (1+Z/10)^{-1/2} \, u(f_0,Z,W) \quad \text{db/Meter} \qquad (34)$$

The conclusion of the calculation of "surface" loss in db/bounce due to bubbles requires integration of Eq. (34 ) over the surface duct ray path of varying curvature and varying attenuation:

$$A_b = 2 \int_L^0 a_b \, ds$$

where L is the depth at which the ray direction is horizontal. Inserting $a_b$ and

$$ds = \frac{dZ}{\sin\theta} \approx \frac{\mathcal{R}\,dZ}{2\sqrt{2\mathcal{R}(L-Z)}} \approx \frac{1}{2}\sqrt{\frac{c}{2(L-Z)G}}\,dZ$$

where $\mathcal{R}$ = local radius of curvature, G(Z) is the total local gradient, and c = local velocity, M/sec, we obtain

$$A_b = 1.06 \times 10^9 \sqrt{c} \int_L^0 \frac{u(f_0,Z,W)\,dZ}{(L-Z)^{1/2}\,(1+0.1Z)^{1/2}\,G^{1/2}(Z)} . \qquad (35)$$

For frequencies below 16 kHz, the expression for the bubble fraction, from Table 2 and Section C, is

$$u(f_0,Z,W) = 0.8 \times 10^{-24} f_0^{3} \beta^{7/2} W [1 + 10^{-2}(W/10)^2] \qquad (36)$$

where $W$ is in knots and $f_0$ is in Hz.

## V. SURFACE DUCT PROPACATION - COMPARISON WITH EXPERIMENT

Bucker[1] has recently solved the surface duct propagation problem by a wave theory approach. His modal components, which correspond to up and down propagating waves, with appropriate ray directions, lose energy when they interact with the surface and by leakage through the thermocline. Our proposal here is to introduce the results of our development in Sections III and IV into Bucker's sclution. Two changes are necessary: the velocity gradient in the duct will now be due to bubbles as well as temperature and pressure effects; the loss at the surface will be made up of the losses per bounce due to below-surface extinction of sound by bubbles and simple, at-surface, coherent specular scatter (because, in general, $g < 1$), calculated for each contributing mode. The surface "reflection coefficient" is thereby directly attributable to the wind velocity which is the sole source of the rms wave height* in the examples chosen and a principal cause of the bubbles.

First, let us look at how the losses vary with wind speed and ray angle of incidence. Our loss calculations are based on eqs. 15, 35, 36. Our ray paths are calculated from the bubble-caused gradient using eqs. 25, 32 together with a temperature plus pressure-caused gradient of 0.048 $sec^{-1}$. Figure 7 illustrates the relative contributions of surface loss and integrated bubble loss for a range of winds with a ray that is horizontal at 40 M, $\varphi = 4.38°$. The frequency is $\sim$ 16 kHz below. It is observed that the bubble contribution dominates only for low wind speeds.

*In the data report[27] the "seaman's eye" estimates of the peak-to-peak wave height, H, are in good (80%) agreement with the calculation from equation (6) when it is assumed that $H = 6\sigma$, for Gaussian wave systems. However, our laboratory experiments suggest that, in general, the total height due to swell and "sea" should be used to determine $\sigma$.

Figure 8 shows that the bubble loss per bounce is not very sensitive to the depth of the horizontal ray (or angle of incidence at the surface); the loss per bounce at the surface, however, increases as the square of the sine of the grazing angle.

For higher frequencies it would be expected that the neglect of the incoherent surface scattering term would no longer be possible; the forward scatter loss would reach an asymptotic value which would be smaller than the increased bubble loss. For frequencies lower than our example the coherent scatter approximation, $e^{-g}$, becomes even better, and would be applicable to higher sea states; the bubble loss would be expected to continue to be smaller than the surface loss.

The experimental propagation data for our study are again from Runs 73 and 99 of the operational tests of the SQS-26 sonar[27] in which both source and receiver were in the duct. The wave heights are such that $g < 1$ for all effective modes of the duct solution.

Since Bucker's duct solution assumes constant velocity gradients, we have had to approximate the calculated total gradient, which goes as $\beta^{-4}$, by splitting it into constant sections $G_1$ and $G_2$ (Fig. 9). The near-surface section, $G_1$, has been given a value twice the uncorrected gradient due to temperature and pressure and the remainder, $G_2$, has been assumed to have no bubble influence. The values are given in Table 3. In this way, the duct propagation loss curves have been recalculated by Bucker. They compare well with the data (Figs. 10, 11). The dashed lines in Figures 10 and 11 are the much poorer predictions based on the equations of project AMOS[28]/

TABLE 3

Data for Two Surface Duct Experiments

| Run No. | $V_s$ | $Z_t$ | $G_1$ | $G_2$ | W |
|---|---|---|---|---|---|
| | M/sec | M | $sec^{-1}$ | $sec^{-1}$ | knots |
| 73 | 1513.1 | 36.6 | 0.096 | 0.048 | 17 |
| 99 | 1510.9 | 51.8 | 0.102 | 0.034 | 15 |

where $V_s$ = velocity at surface

$Z_t$ = depth of thermocline

$G_1$ = velocity gradient, surface to 8 yards

$G_2$ = velocity gradient, 8 yards to thermocline

Other, higher values of the assumed bilinear gradient and a closer-fitting tri-linear gradient have also been considered. However, the resulting propagation prediction curves show excessive losses compared to experiment. Since, at these wind speeds, the bubble loss is less than the surface loss, the velocity gradient can be a major influence. This suggests that our total bubble populations, $U(f_0,Z,W)$, may be too high, perhaps by a factor of two, possibly due to the wrong wind speed dependence having been assumed.

## VI. CONCLUSION

The purpose of this paper has been to show that for a large range of ocean surface roughness, $g < 1$, it is possible to predict surface duct propagation by using the simplest surface scattering theory (coherent term only) and estimates of bubble presence as inputs to the Bucker modal solution.

Nevertheless, it is the necessity of knowing more about the ocean parameters of sound propagation that has been demonstrated by this paper. It is hoped that the present work will serve as a spur for more fundamental studies to replace the speculative assumptions that we have been forced to make about bubble dependence on wind speed.

## VII. ACKNOWLEDGEMENT

The author is indebted to Homer R. Bucker and Burton Hurdle for several stimulating discussions which contributed significantly to this paper. It was Morris Schulkin who urged us to bring the bubble work to print; his encouragement is much appreciated. Computer services were provided by the Naval Research Laboratory and Mrs. Rosemary Lande of the Ocean Physics Group of the Naval Postgraduate School. This research was partially supported by Naval Ship Systems Command.

## REFERENCES


1. Bucker, H. P., "Wave Theory Solution for Sound Propagation in a Surface Duct with Rough Surface", J. U. A. (USN) 19, 13-28 (1969) (Confidential).

2. W. J. Pierson Jr., and L. Moskowitz, "A Proposed Spectral Form for Fully Developed Wind Seas Based on the Similarity Theory of S. A. Kitaigorodskii." J. Geophys. Res., 69, 5181-5190. (1964).

3. C. Cox and W. Munk, "Measurement of the Roughness of the Sea Surface from Photographs of the Sun's Glitter." J. Opt. Soc. Am. 44, 838-850 (1954).

4. W. J. Pierson, Jr., "The Interpretation of Wave Spectrums in Terms of the Wind Profile Instead of the Wind Measured at a Constant Height." J. Geophys. Res, 69, 5191-5203 (1964).

5. P. Beckmann and A. Spizzichino, "The Scattering of Electromagnetic Waves from Rough Surfaces", MacMillan Co., New York. (1963)

6. H. Medwin, "Specular Scattering of Underwater Sound from a Wind-Driven Surface," J. Acoust. Soc. Am. 41, 1485-1495. (1967)

7. Yu. Yu. Zhitkovskiy and Yu. P. Lysanov, "On Certain Features of the Fresnel Diffraction of Sound on the Agitated Surface and on the Bottom of the Ocean." Izvestiya, Atmospheric and Oceanic Physics, 5, 556-568 (1969).

8. C. W. Horton, Sr. and D. R. Melton, "Importance of the Fresnel Correction in Scattering from a Rough Surface, II. Scattering Coefficient", J. Acoust. Soc. Am., 47, 299-303. (1970)

9. G. R. Barnard et al., "Underwater-Sound Reflection From a Pressure-Release Sinusoidal Surface," J. Acoust. Soc. Am. 39, 1162-1169. (1966)

10. H. Medwin and C. S. Clay, "Dependence of Spatial and Temporal Correlation of Forward-Scattered Underwater Sound on the Surface Statistics - Part II Experiment," J. Acoust. Soc. Am., 48 , 1419-1429. (1970)

11. J. Scheible, R. Fowler and H. Medwin, "Near-Grazing Specular Scatter of Underwater Sound From a Wind-Driven Model Sea Surface," J. Acoust. Soc. Am. 44, 355. (1968) Abstract.

12. N. Mayo, H. Medwin and W. Wright., "Specular Scattering of Underwater Sound from Anisotropic Sea and Swell Surfaces," [illegible] J. Acoust. Soc. Am. 47, 112. (1970) Abstract.

13. Blanchard, D. C. and A. H. Woodcock , "Bubble Formation and Modification in the Sea and its Meteorological Significance", Tellus 9, 145-158. (1957)

14. Glotov, V. P. et al.,"Investigation of the Scattering of Sound by Bubbles Generated by an Artificial Wind is Sea Water and the Statistical Distribution of Bubble Sizes", Sov. Phys. Acoust. 7, 341-345. (1962)

15. Schulkin, M., "Surface Coupled Losses in Surface Sound Channel Propagation II", J. Acoust. Soc. Am., 45, 1054-1055. (1969)

16. Medwin, H., "In Situ Acoustic Measurements of Bubble Populations in Coastal Ocean Waters", J. Geoph. Res. 75, 599-611. (1970).

17. Monahen, E. C. and C. R. Zietlow, "Laboratory comparisons of Fresh-Water and Salt-Water Whitecaps", J. Geoph. Res. 74, 6961-6966. (1969)

18. Gavrilov, L. R. , "On the Size Distribution of Gas Bubbles in Water", Sov. Phys. Acoust. 15, 22-24. (1969)

19. Messino, D.,D. Sette and F. Wanderlingh,"Statistical Approach to Ultrasonic Cavitation", J. Acoust. Soc. Am. 35, 1575-1583. (1963)

20. Sirotyuk, M. G., "Experimental Ultrasonic Cavitation Studies" in Physics and Technology of High Intensity Ultrasonics" (In Russian) L.D. Rozenberg, ed. Vol. 2. of "Nauka", Moscow, 1968.

21. Blanchard, D. C., "The Electrification of the Atmosphere by Particles from Bubbles in the Sea", Progress in Oceanography 1, 71-202. MacMillan Co., New York City, 1963.

22. O. M. Phillips, "The Dynamics of the Upper Ocean", Cambridge University Press, London. (1966).

23. Shonting, D. H., "Autospectra of Observed Particle Motions of Wind Waves", J. Mar. Res. 26, 43-65. (1968)

24. S. Tabata, N.E.J. Boston and F.M. Boyce, "The Relation Between Wind Speed and Summer Isothermal Surface Layer of Water at Ocean Sta ion P in the Eastern Subarctic Pacific Ocean", J. Geophys. Res. 70, 3867-3878. (1965)

25. Morse, P. M. and H. Feshbach , "Methods of Theoretical Physics", Vol. II, p. 1498, Published by McGraw Hill Book Co., New York City, 1953.

26. N.D.R.C. Summary Technical Report of Div. 6. Vol. 8, p. 470. Washington, D.C., 1946.

27. C.H. Wiseman, Cdr. USN, "Comparison of Observed and Predicted Underwater Acoustic Propagation loss (U)", Key West Test and Evaluation Detachment Report (28 Nov. 1967).

28. H. W. Marsh and M. Schulkin "Report on the Status of Project AMOS (Acoustical, Meteorological and Oceanographic Survey) (1 Jan 1953-Dec 1954) USN Underwater Sound Lab. Report 255A, 1-82 (1967).

## LIST OF FIGURES

## LIST OF TABLES

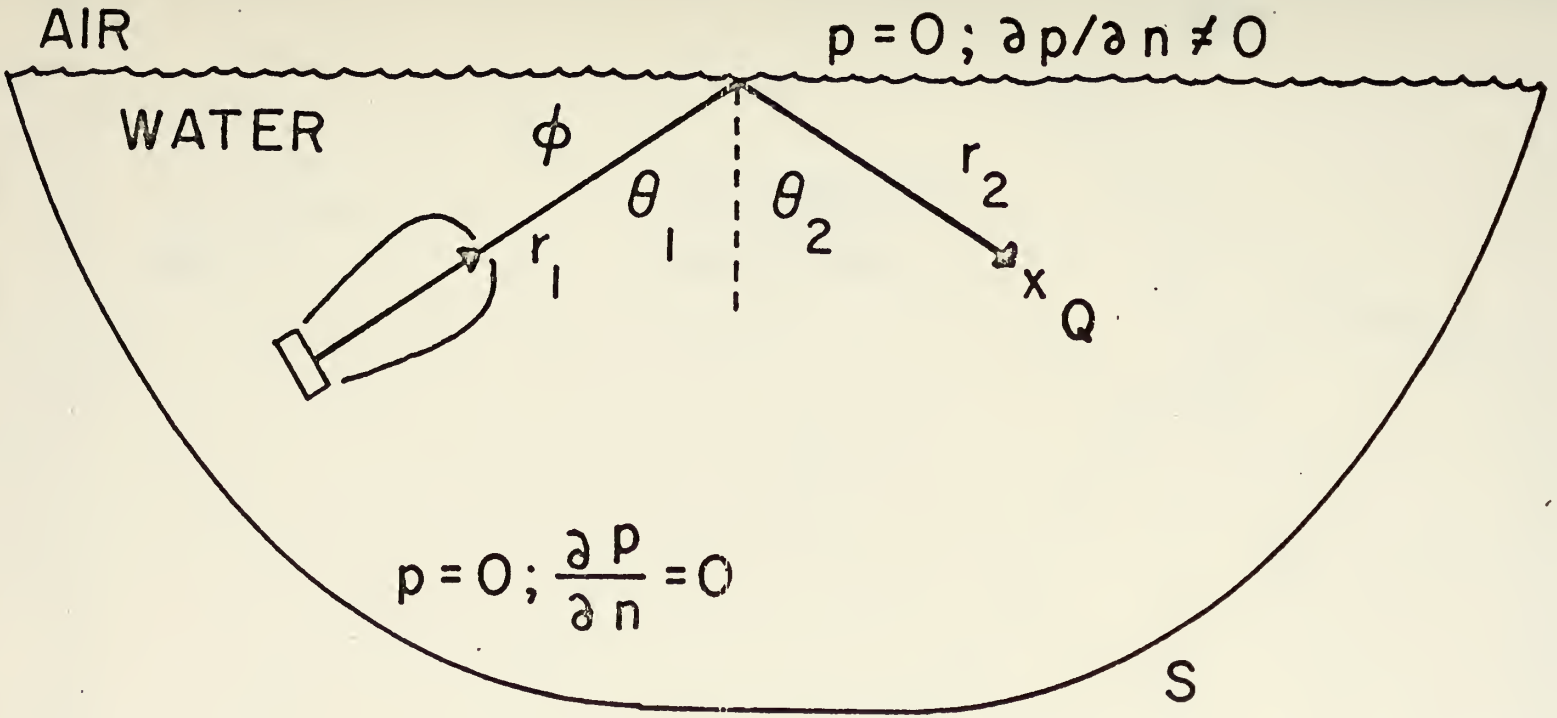


Scattering Geometry

FIG 1

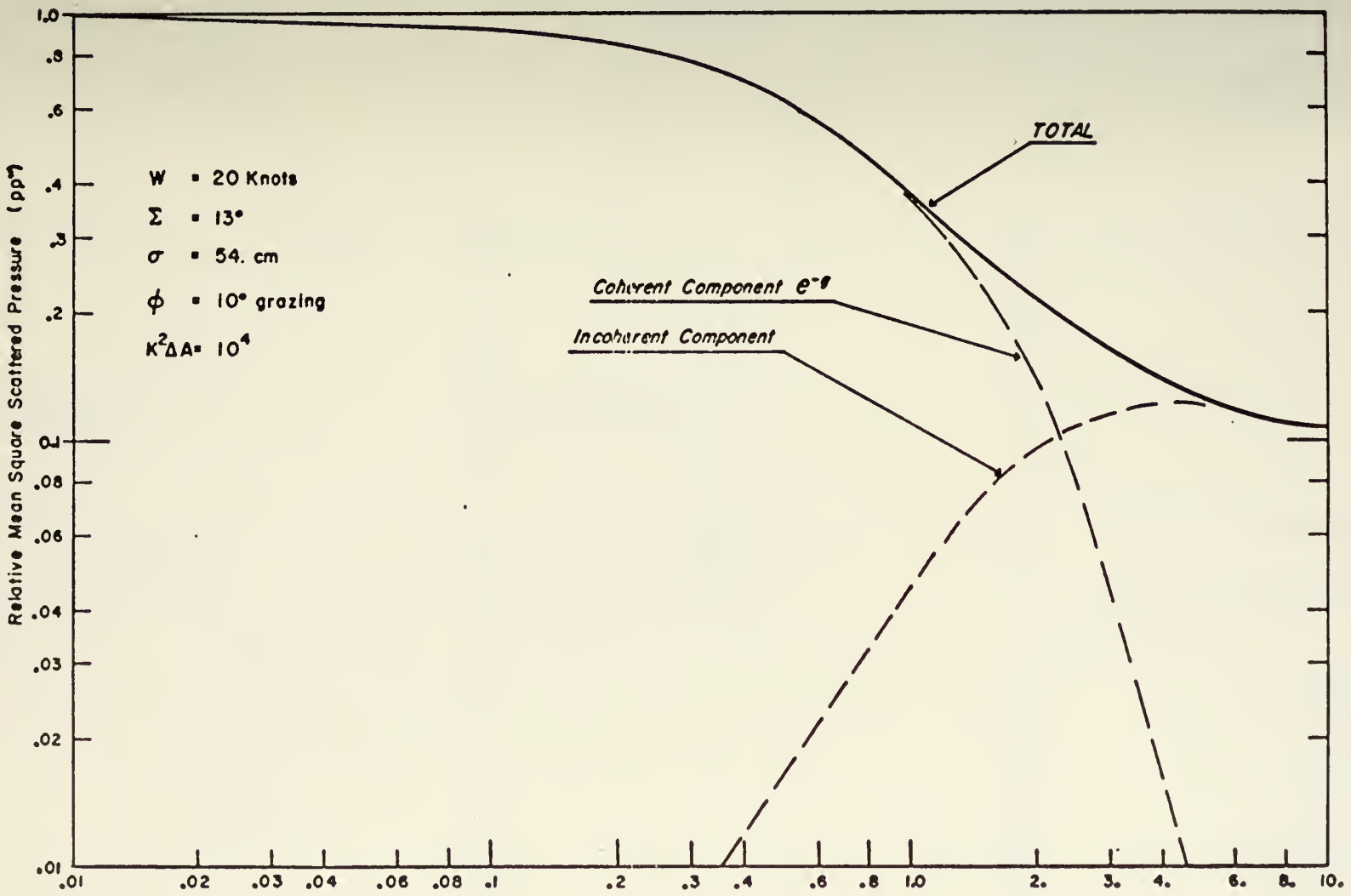


Typical Behavior of Coherent and Incoherent Components in Specular Scatter.

$$g = \frac{16\pi^2\sigma^2}{\lambda^2}\sin^2\phi = \text{Acoustical Roughness}$$

F162

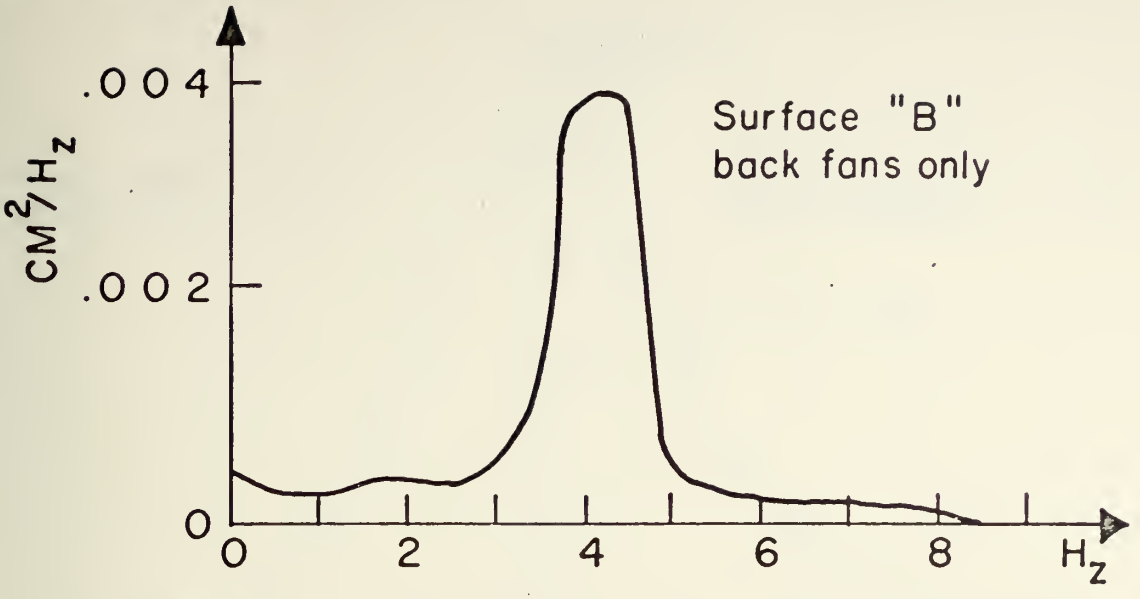
.004
.002
0
$CM^2/H_z$
Surface "B"
back fans only
0
2
4
6
8
$H_z$

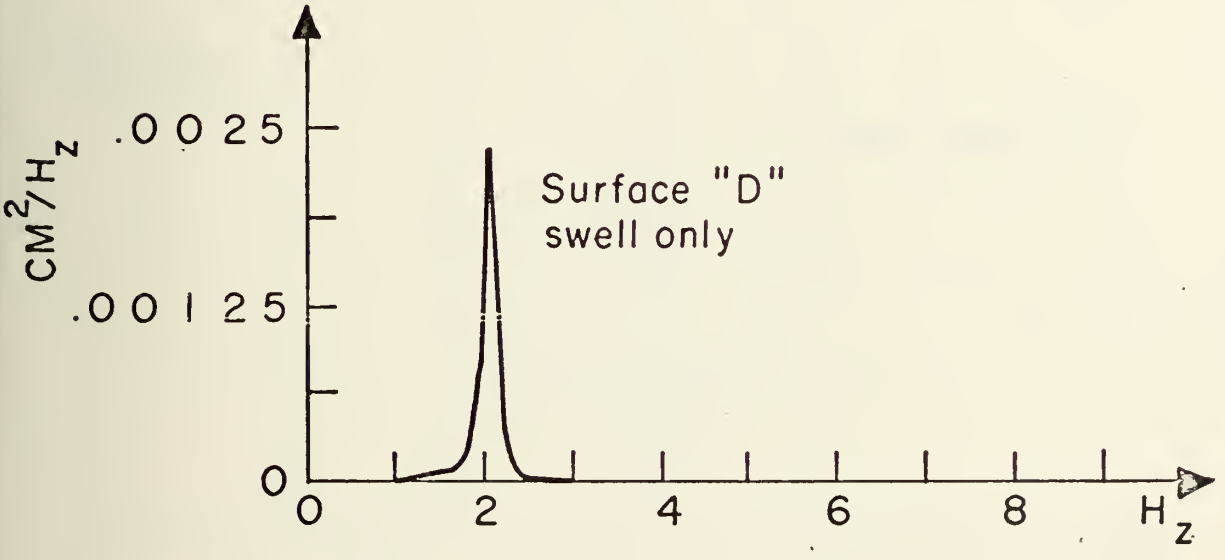
.0025
.00125
0
$CM^2/H_z$
Surface "D"
swell only
0
2
4
6
8
$H_z$

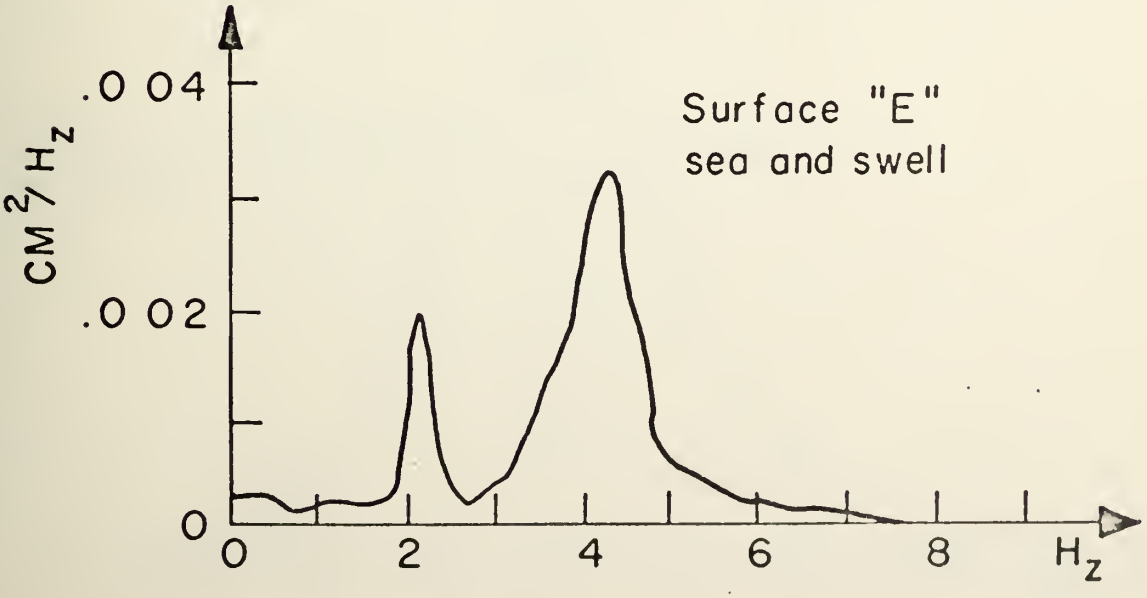
.004
.002
0
$CM^2/H_z$
Surface "E"
sea and swell
0
2
4
6
8
$H_z$

FIG 3

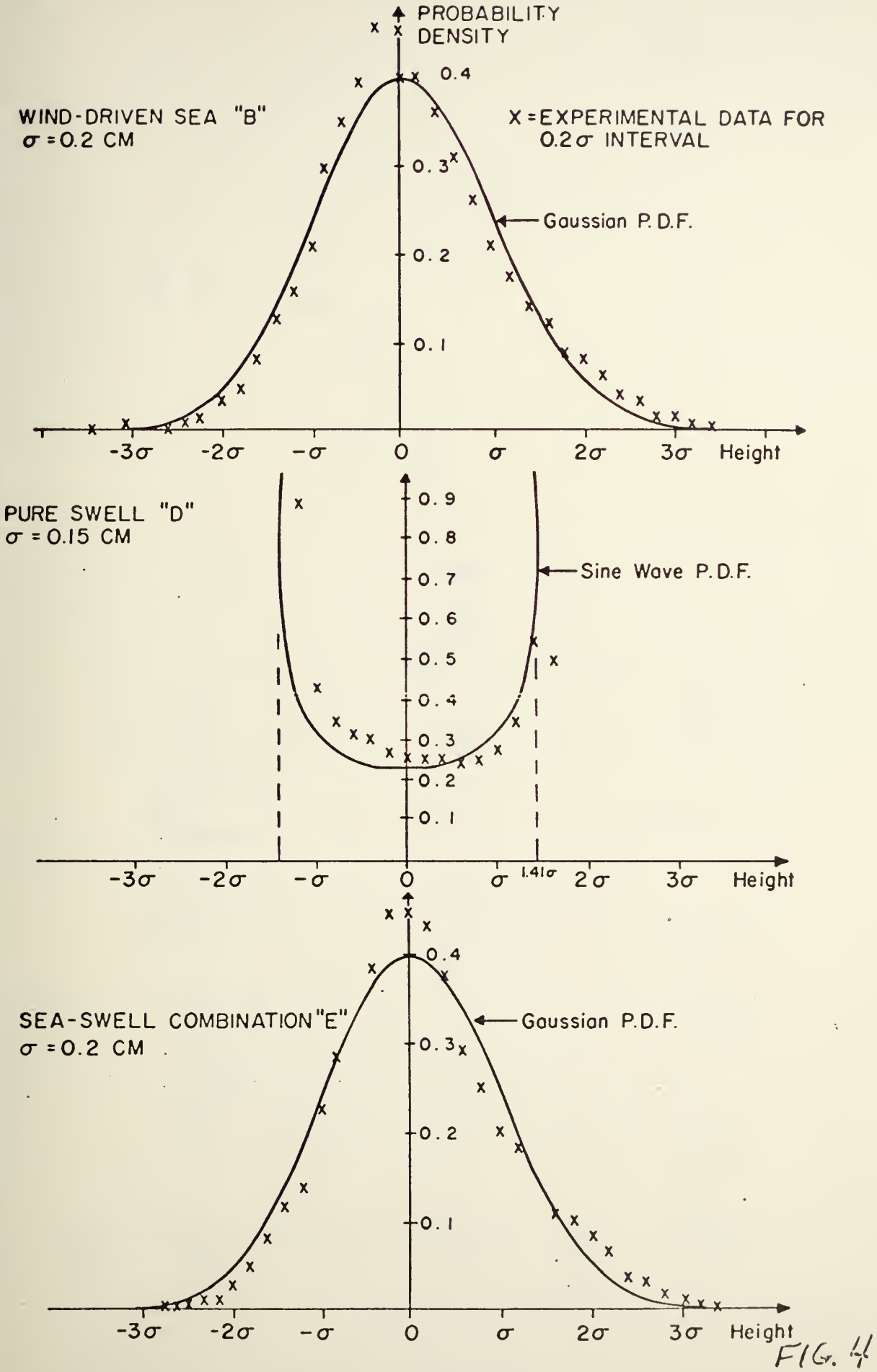
PROBABILITY DENSITY
WIND-DRIVEN SEA "B"
σ = 0.2 CM
X = EXPERIMENTAL DATA FOR 0.2σ INTERVAL
Gaussian P.D.F.
0.4
0.3
0.2
0.1
-3σ
-2σ
-σ
0
σ
2σ
3σ
Height
PURE SWELL "D"
σ = 0.15 CM
Sine Wave P.D.F.
0.9
0.8
0.7
0.6
0.5
0.4
0.3
0.2
0.1
1.41σ
SEA-SWELL COMBINATION "E"
σ = 0.2 CM
Gaussian P.D.F.

FIG. 4

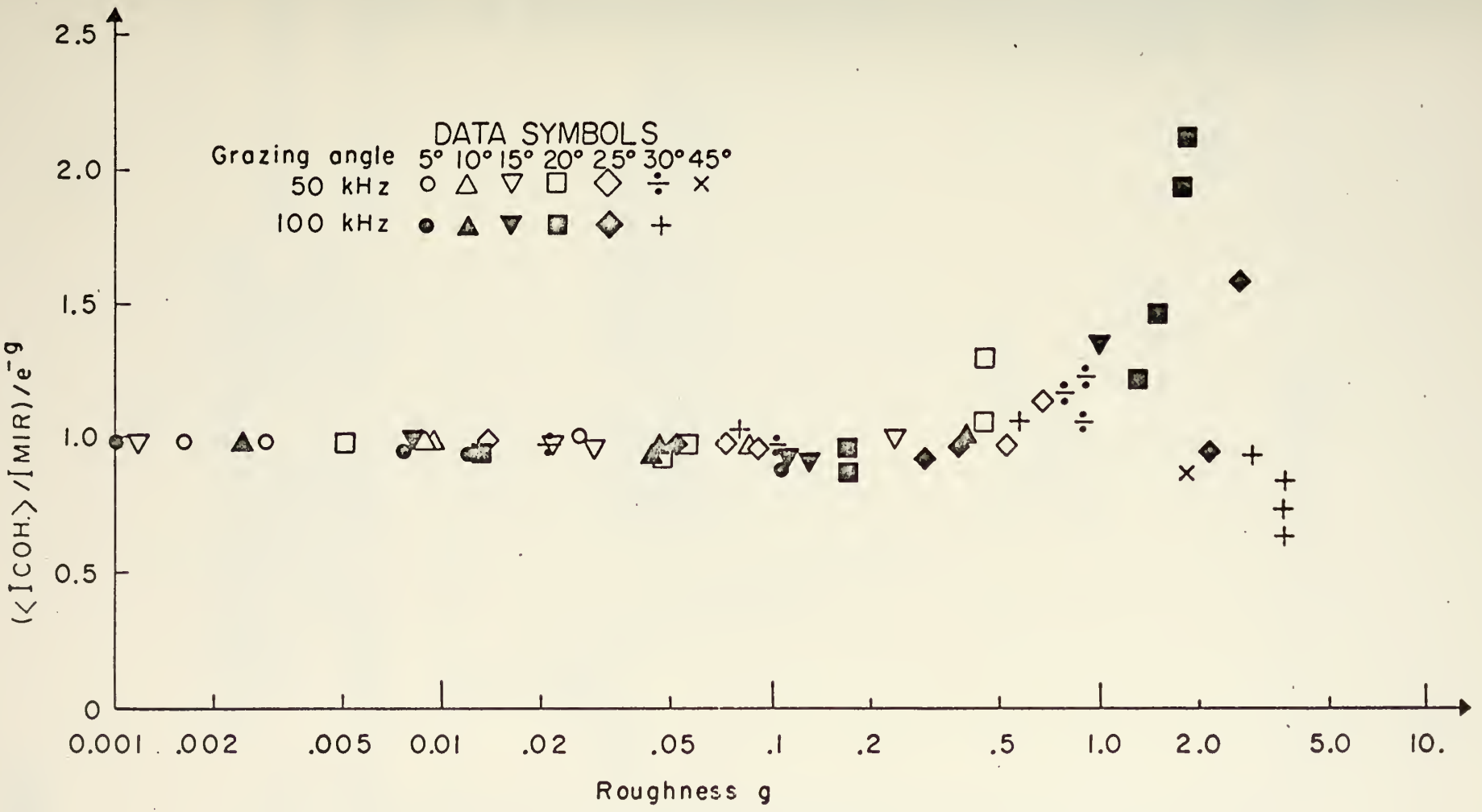
DATA SYMBOLS
Grazing angle 5° 10° 15° 20° 25° 30° 45°
50 kHz
100 kHz
2.5
2.0
1.5
1.0
0.5
0
(<ICOH.>/[MIR])/e^-g
0.001
.002
.005
0.01
.02
.05
.1
.2
.5
1.0
2.0
5.0
10.
Roughness g

FIG5

Fig. 6

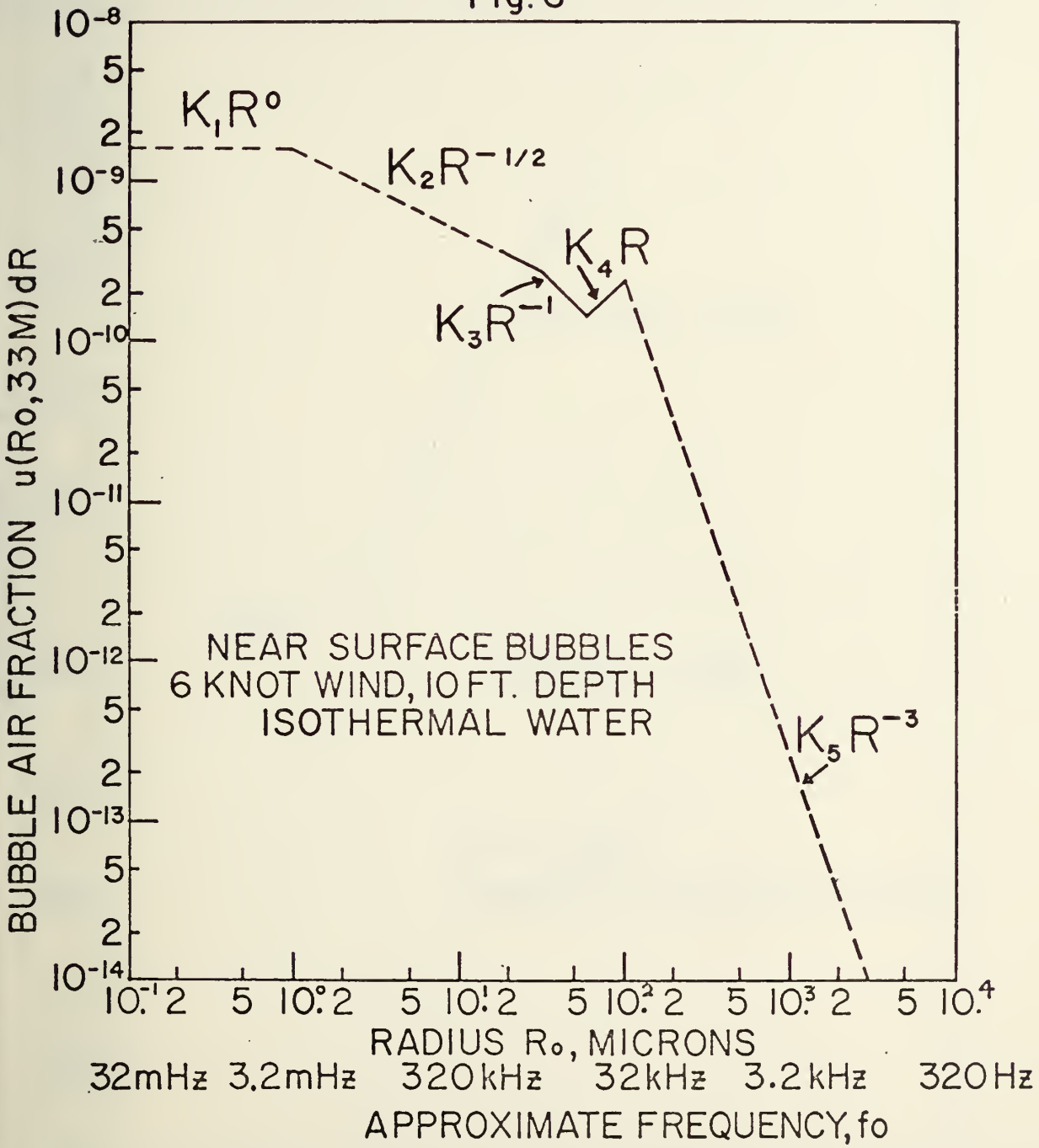
$K_1R^0$
$K_2R^{-1/2}$
$K_3R^{-1}$
$K_4R$
$K_5R^{-3}$
NEAR SURFACE BUBBLES
6 KNOT WIND, 10 FT. DEPTH
ISOTHERMAL WATER
BUBBLE AIR FRACTION u(Ro,33M)dR
$10^{-8}$ 5 2 $10^{-9}$ 5 2 $10^{-10}$ 5 2 $10^{-11}$ 5 2 $10^{-12}$ 5 2 $10^{-13}$ 5 2 $10^{-14}$
$10^{-1}$ 2 5 $10^{0}$ 2 5 $10^{1}$ 2 5 $10^{2}$ 2 5 $10^{3}$ 2 5 $10^{4}$
RADIUS Ro, MICRONS
32mHz 3.2mHz 320kHz 32kHz 3.2kHz 320Hz
APPROXIMATE FREQUENCY, fo

FIG 6

FIG.7

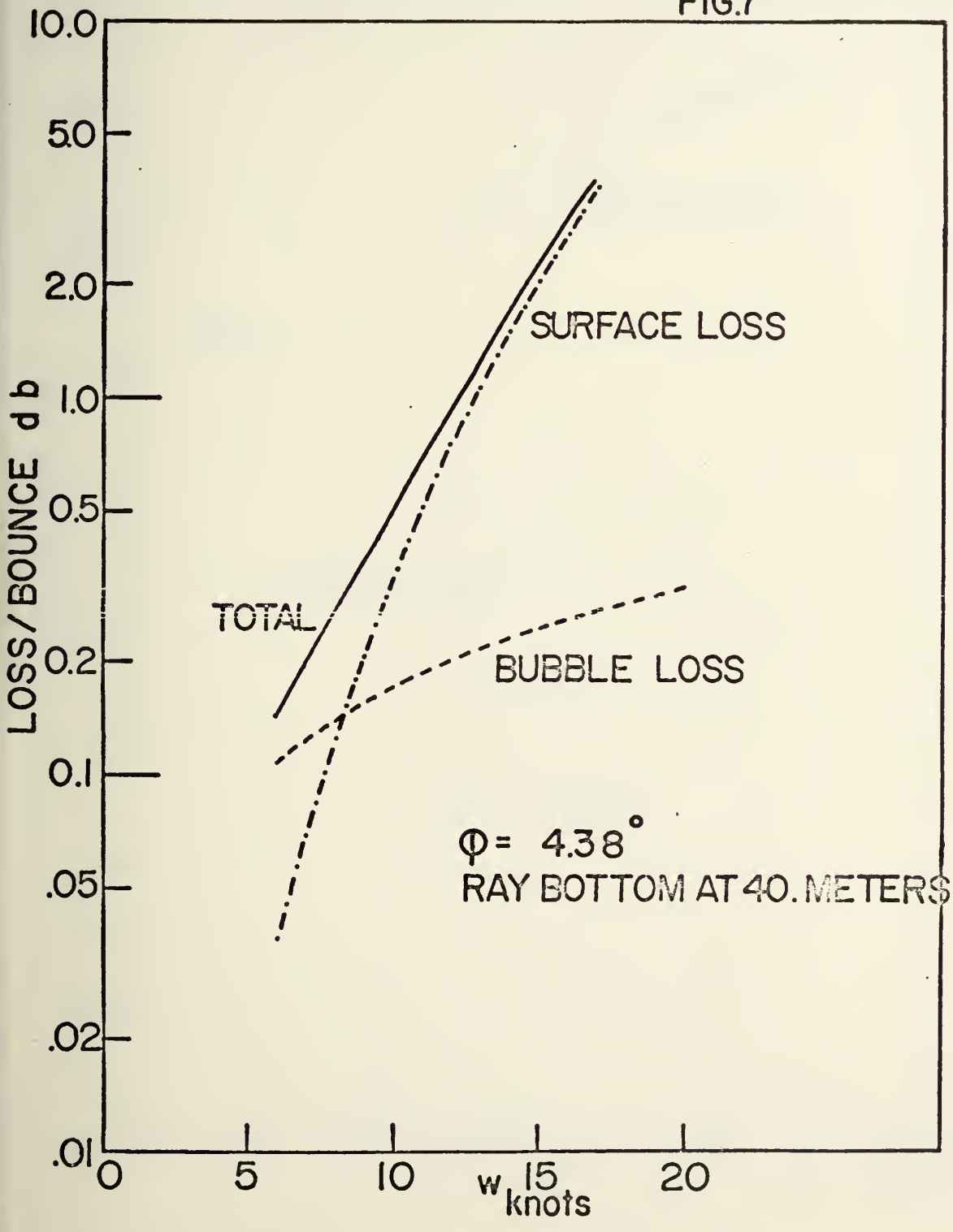
10.0
5.0
2.0
1.0
0.5
0.2
0.1
.05
.02
.01
LOSS/BOUNCE d b
SURFACE LOSS
TOTAL
BUBBLE LOSS
Φ= 4.38°
RAY BOTTOM AT 40. METERS
0
5
10
15
20
w knots

FIG 7

FIG.8

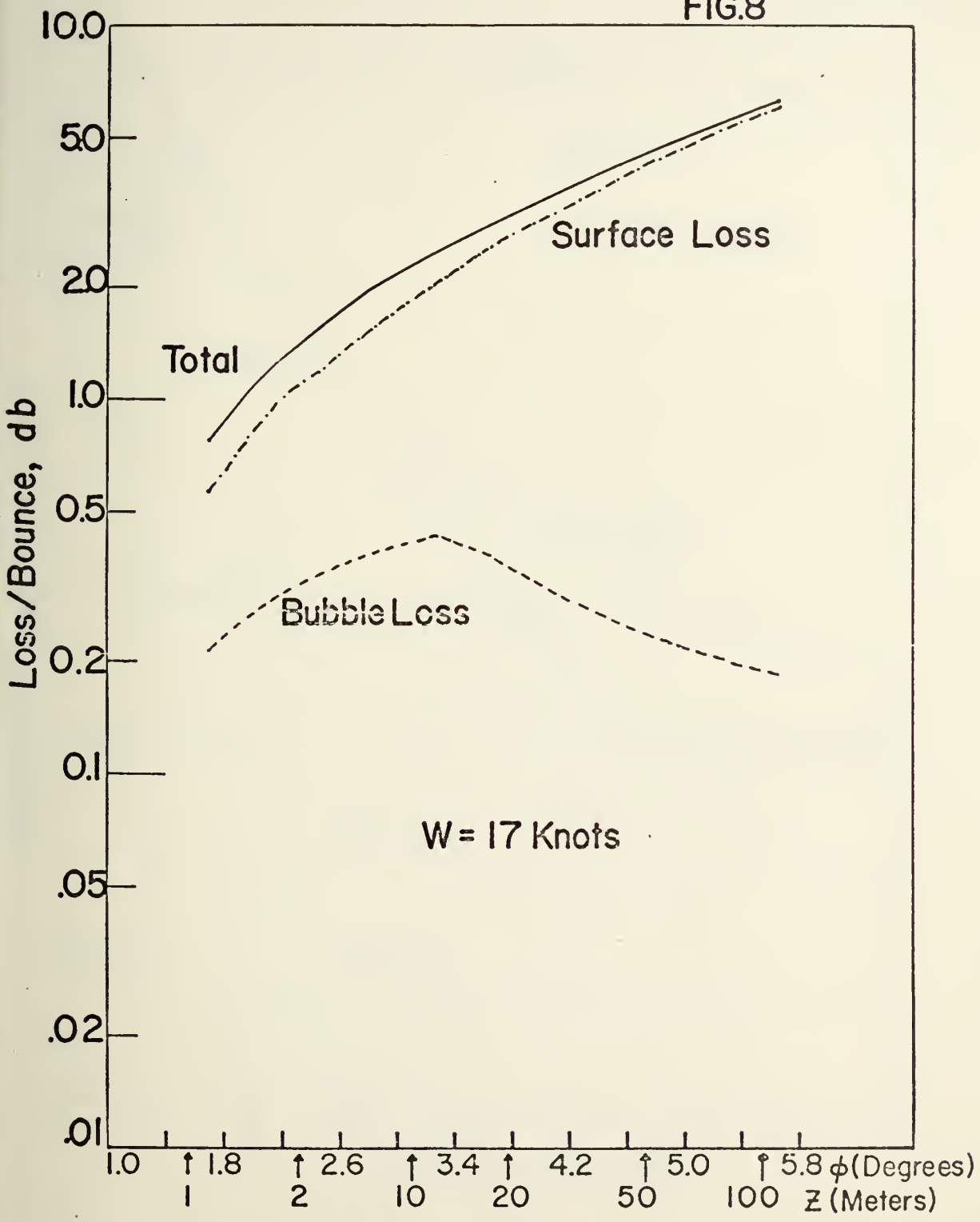
10.0
5.0
2.0
1.0
0.5
0.2
0.1
.05
.02
.01
Loss/Bounce, db
Surface Loss
Total
Bubble Loss
W = 17 Knots
1.0
1.8
2.6
3.4
4.2
5.0
5.8 φ(Degrees)
1
2
10
20
50
100 Z (Meters)

FIG 8

FIG. 9

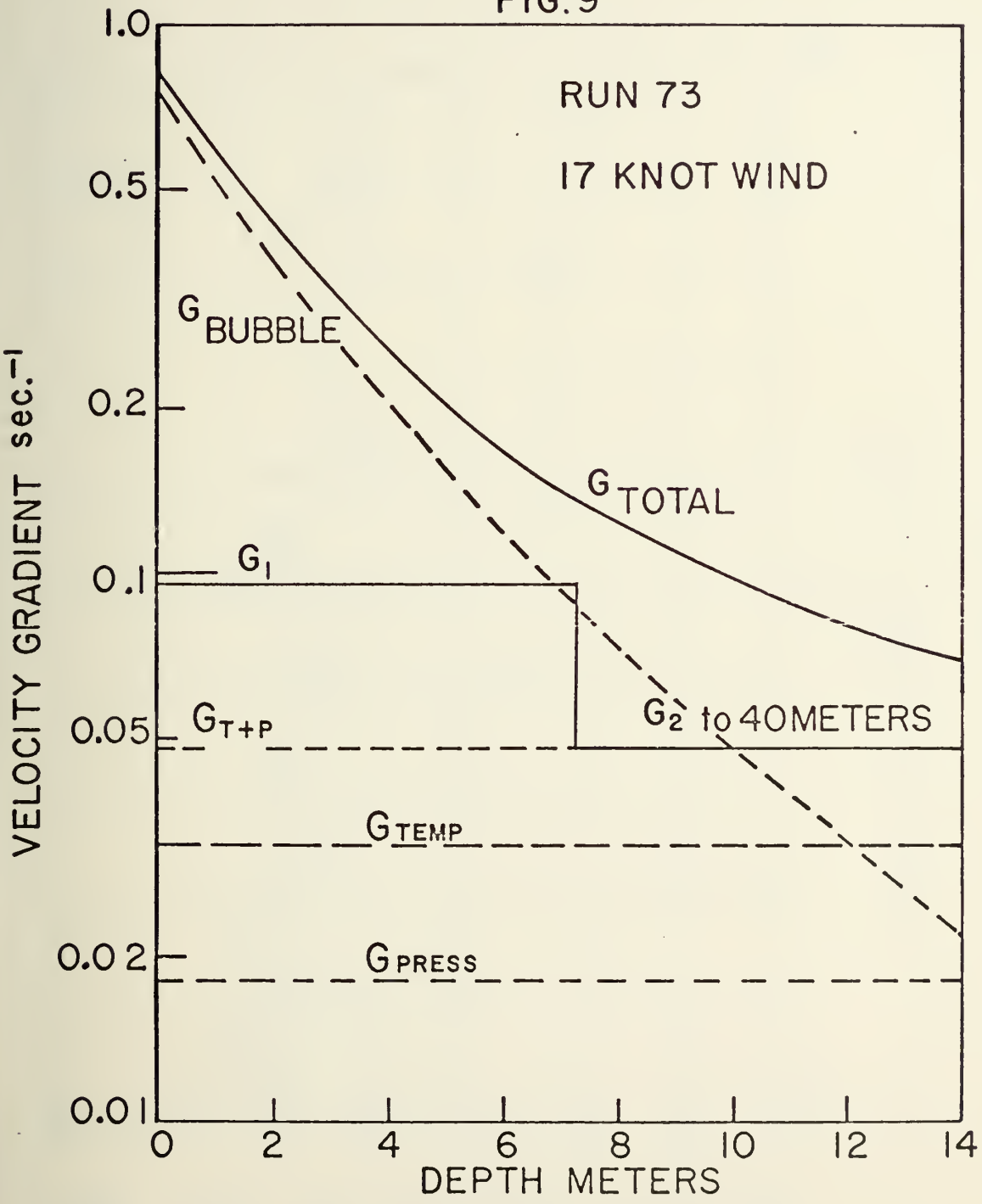
RUN 73
17 KNOT WIND
G BUBBLE
G TOTAL
G1
G2 to 40METERS
GT+P
GTEMP
GPRESS
VELOCITY GRADIENT sec.-1
1.0
0.5
0.2
0.1
0.05
0.02
0.01
0
2
4
6
8
10
12
14
DEPTH METERS

FIG 9

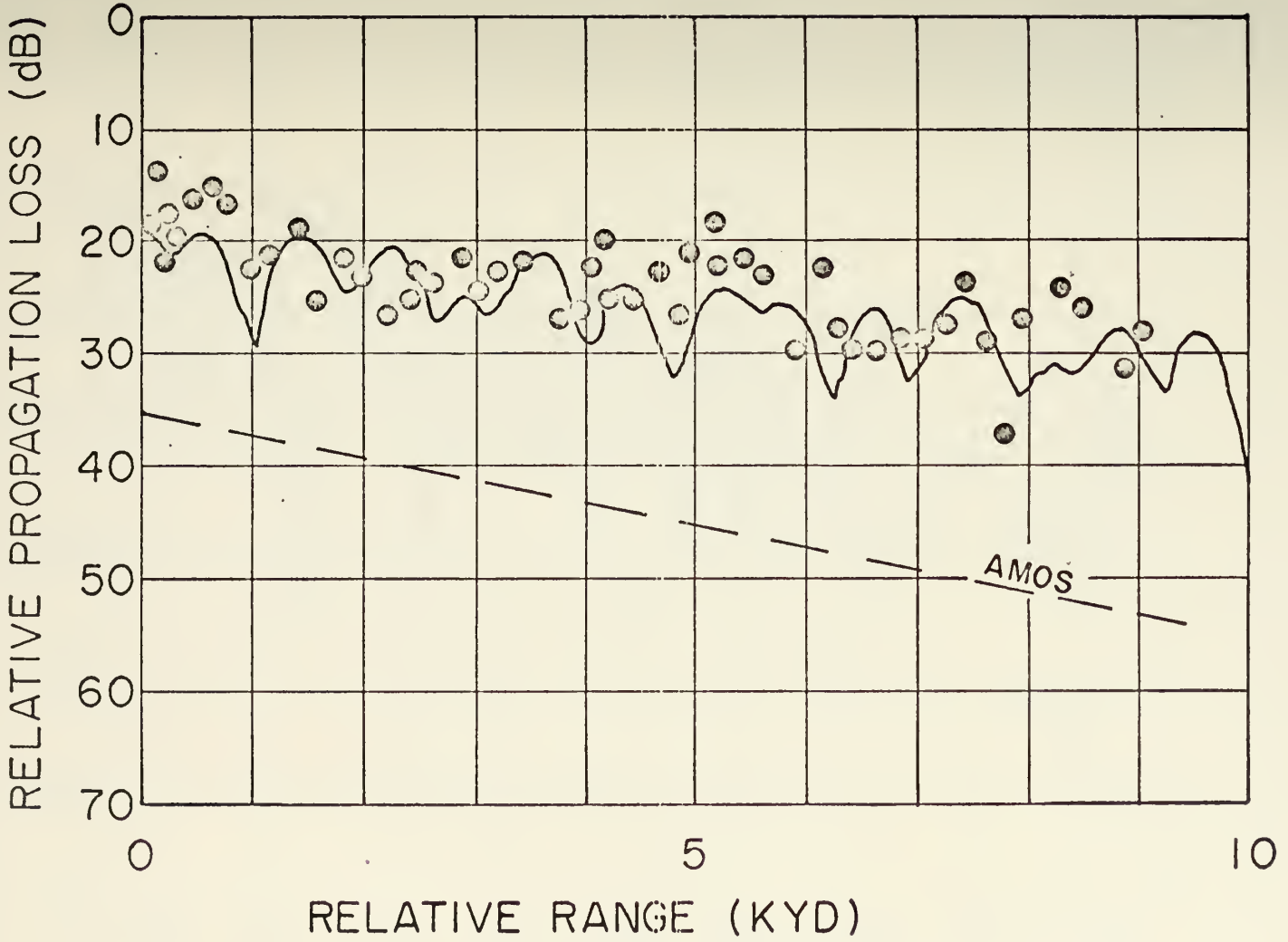
RELATIVE PROPAGATION LOSS (dB)
0
10
20
30
40
50
60
70
AMOS
0
5
10
RELATIVE RANGE (KYD)

FIG. 10

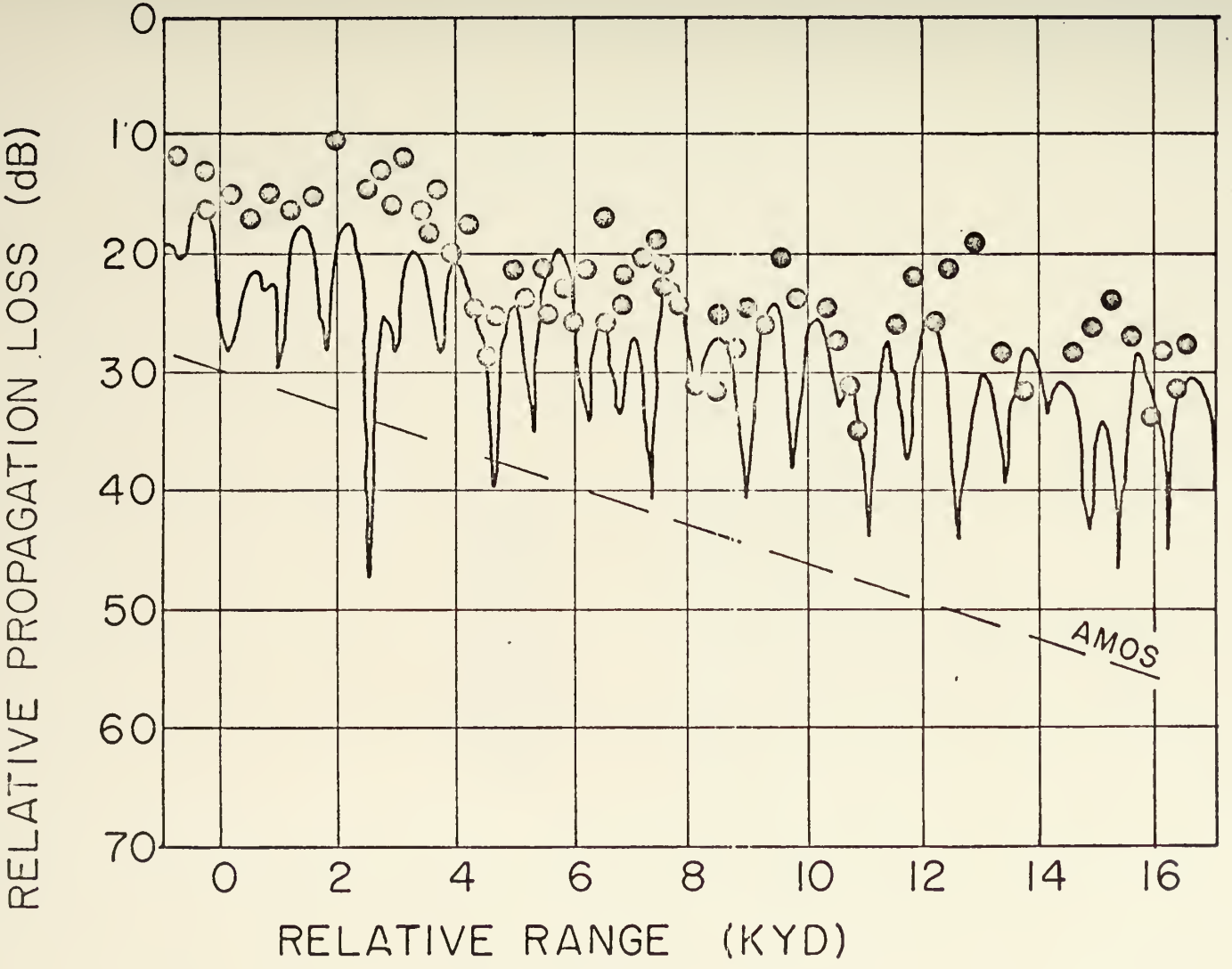
RELATIVE PROPAGATION LOSS (dB)
0
10
20
30
40
50
60
70
0
2
4
6
8
10
12
14
16
RELATIVE RANGE (KYD)
AMOS

FIG. 11